Instantaneous Frequency Estimation Methods of Micro-Doppler Signal

Lingxiao Li*, **Zhixing Huang, and Wei Zhang**

Abstract—Extracting instantaneous frequency (IF) of Micro-Doppler (M-D) is the key to estimating micro-motion parameters. In this paper, firstly, the micro-motion model of coning was set up. Meanwhile, the theoretical analysis and derivation of micro-Doppler were performed. Then we introduced occlusion effect and Time Frequency transform to better accord with the complexity and reality of feature extraction of Micro-Doppler in the real world. Besides other computational complex separation methods, we extended the Viterbi algorithm for some cases and proposed two novel means, selecting local maximum value and extracting central position, to solve the dilemma where the Viterbi algorithm failed. Finally corresponding simulation corrected the performance of the two methods in different Signal to Noise Ratio (SNR). The simulation analysis showed that the methods were effective if time-frequency map was not polluted seriously by noise.

1. INTRODUCTION

In recent years, micro-Doppler effect of radar target has become a research focus in the field of target feature extraction and recognition. It is assured that target recognition technology based on the micro-Doppler features of object is one of the most promising technologies of radar [1].

In 2000, Chen first introduced the concept of micro-Doppler from laser radar to the microwave radar. Then he elaborated this concept in the literature [2], modeling basic micro motion and extracting features from micro-Doppler signatures with the utilization of time-frequency analysis method. So far, there have been a large number of scholars have achieved a lot in the micro-Doppler feature extraction on the above basis [3–10]. However, time-frequency analysis is still the main means of target micro-Doppler extraction. Due to the uncertainty principle limitation, the time-frequency map cannot focus in the frequency domain, as well as unable to locate the micro-Doppler frequency uniquely. Literature [11] proposed a peak detection method and the first-order time conditional moment method to extract the micro Doppler frequency distribution curve, but only the case of single target with a single micro-scatter was analyzed. When it comes to the cases of multiple targets in a resolution cell or multiple scatters on the target, the above two methods fail. But many sophisticated separation methods of micro-Doppler signals have been proposed [12–18]. In [12], the micro-Doppler signals were separated by parameterizing into chirplet function. And classical Hough and its extended transform were applied to solve the dilemma [13]. Furthermore, the commonly complex-empirical mode decomposition (CEMD) extended from empirical mode decomposition (EMD) was utilized in feature extraction [14]. Those methods involving complex transform are all computationally exhaustive due to several dimensions optimizations. In this paper, Viterbi algorithm was adopted to separation because of its tracking functionality and comparable simpleness. Taking time complex into consideration, we extended the Viterbi Algorithm within iteration. In the case of occlusion effect, we also proposed two novel frequency curve extraction methods.

* Corresponding author: Lingxiao Li (xiaohunlt@126.com).
The authors are with the Research Institute of Electronic Science and Technology of UESTC, Chengdu 611731, China.

This paper, taking cone rotating target for example, first modeled coning and derived its mathematical model (Section 2). Followed in order of frequency distribution of multiple scatters utilizing STFT (Short Time Frequency Transform) tools (Section 3) and occlusion effect (Section 4), the extended Viterbi Algorithm and two novel frequency curve extraction methods for multi-component case were proposed (Section 5). Eventually, simulation proved the correction of those new algorithms (Section 6).

2. FEATURE ANALYSIS OF CONNING TARGET

2.1. The Concept of Micro-Doppler

The presence of target radial movement (translation) relative to the radar will modulate the carrier frequency of the radar echo, which is commonly known as Doppler Effect. If in the same time the target itself or the structure on it has micro motion (such as vibration, rotation, rolling cone rotation, swing, precession and nutation, etc.), a modulated radar echo with sidebands on the target Doppler frequency will occur. Modulation caused by micro motion is called micro-Doppler phenomenon.

Similar micro-Doppler analysis of different forms of micro-motion model is built differently. For simplicity, here we only took the cone rotating target for example to establish its motion model and to analyze the micro-Doppler features.

2.2. The Micro-Doppler of Coning Target

Figure 1 presents coning target motion model, in which **SN** is precession axis, (x, y, z) as the target local coordinate system, **SN** and the z-axis intersect at point S; (U, V, W) as the radar coordinate system; (X, Y, Z) as the target reference coordinate system. S is the coordinate origin, and the reference coordinate system is parallel to the radar coordinate system. In the radar coordinate system, azimuth and elevation angles of target are α and β, respectively, and for precession axis **SN** in the reference coordinate system, its azimuth and elevation angles are α_N and β_N, respectively.

Therefore, the unit vector of radar line of sight (LOS): $\mathbf{n} = [\cos\alpha\cos\beta, \sin\alpha\cos\beta, \sin\beta]^T$. The unit vector of **SN** axis precession: $\mathbf{e} = [\cos\alpha_N\cos\beta_N, \sin\alpha_N\cos\beta_N, \sin\beta_N]^T$. Assume that the coordinate of target scattering point P is $\mathbf{r}_0 = [x, y, z]^T$ in the local coordinate system. Due to the initial angle (ϕ, θ, φ), rotation matrix of the target in the initial time is:

$$R_{init} = \begin{bmatrix} \cos\phi & -\sin\phi & 0 \\ \sin\phi & \cos\phi & 0 \\ 0 & 0 & 1 \end{bmatrix} \begin{bmatrix} 1 & 0 & 0 \\ 0 & \cos\theta & -\sin\theta \\ 0 & \sin\theta & \cos\theta \end{bmatrix} \begin{bmatrix} \cos\psi & -\sin\psi & 0 \\ \sin\psi & \cos\psi & 0 \\ 0 & 0 & 1 \end{bmatrix} \quad (1)$$

It is easy to obtain that the position of point P in the reference coordinate system is $\mathbf{R}_{inint}\mathbf{r}_0$. Assume that the target rotating around the precession axis has the angular velocity ω (rad/s), according to Rodrigues rotation formula, in time t rotation matrix under the reference coordinate system $(X, Y,$
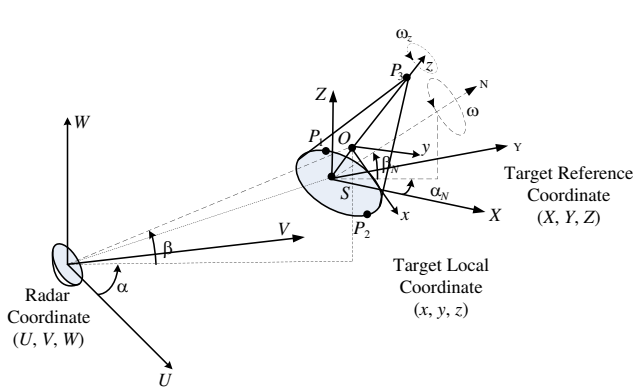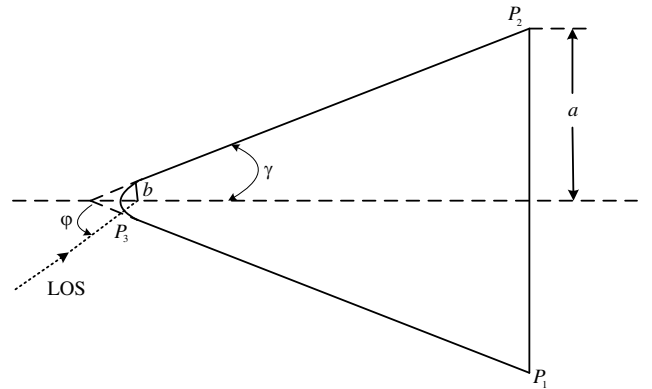

Figure 1. Coning target motion model.

Figure 2. RCS of the coning model.

Z) as:

$$R_t = I + \hat{E}\sin\omega t + \hat{E}^2(1 - \cos\omega t) \tag{2}$$

where **I** is the identity matrix, $\hat{E}$ the skew symmetric matrix and defined as:

$$\hat{E} = \begin{bmatrix} 0 & -\sin\beta_N & \sin\alpha_N\cos\beta_N \\ \sin\beta_N & 0 & -\cos\alpha_N\cos\beta_N \\ -\sin\alpha_N\cos\beta_N & \cos\alpha_N\cos\beta_N & 0 \end{bmatrix} \tag{3}$$

So in the instant t, the displacement between point P and origin in reference coordinates is $\mathbf{r}(t) = R_t \cdot R_{init} \cdot [x, y, z - z_0]^T$. Supposing that the initial position of S point in the radar coordinates is $\mathbf{R}_o$, the radial velocity of the target is $\mathbf{V}$, which can get $R(t)$, the position of the point P on time t in the radar coordinate system. $\mathbf{R}(t) = \mathbf{R}_o + \mathbf{V} \cdot t + \mathbf{r}(t)$. The distance between target and radar satisfied $R(t) = \|\mathbf{R}(t)\|_2 = \|\mathbf{R}_0 + \mathbf{V}t + \mathbf{r}(t)\|_2$. The phase transformation caused by $R(t)$ is:

$$\Phi[R(t)] = 2\pi f \frac{2R(t)}{c} \tag{4}$$

where f is the radar carrier frequency and c the speed of light.

So the target Doppler frequency is:

$$f_D = \frac{1}{2\pi}\frac{d\Phi[R(t)]}{dt} = \frac{2f}{c}\frac{d}{dt}R(t) = \frac{2f}{c}\frac{1}{2R(t)}\frac{d}{dt}\left[(\mathbf{R}_o + \mathbf{V}\cdot t + \mathbf{r}(t))^T \cdot (\mathbf{R}_o + \mathbf{V}\cdot t + \mathbf{r}(t))\right]$$

$$= \frac{2f}{c}\left[\mathbf{V} + \frac{d}{dt}\mathbf{r}(t)\right]^T \mathbf{n}_p \tag{5}$$

where the unit vector of the point P in the radar coordinate system, $\mathbf{n}_p$, is $\mathbf{n}_p = (\mathbf{R}_o + \mathbf{V}\cdot t + \mathbf{r}(t))/\|\mathbf{R}_o + \mathbf{V}\cdot t + \mathbf{r}(t)\|_2$. When t is small, $\|\mathbf{R}_0\| \gg \|\mathbf{V}\cdot t + \mathbf{r}(t)\|$, $\mathbf{n}_p$ can be approximated to $\mathbf{n}$. Then

$$f_D = \frac{2f}{c}\left[\mathbf{V} + \frac{d}{dt}\mathbf{r}(t)\right]^T \mathbf{n} = \frac{2f}{c}\left[\mathbf{V} + \frac{d}{dt}\mathbf{r}(t)\right]_{\text{radial}} \tag{6}$$

From the above equation, the first part $\frac{2f}{c}[\mathbf{V}]_{\text{radial}}$ is induced by translation, while the latter is caused by coning:

$$f_{\text{micro-Doppler}} = \frac{2f}{c}\left[\frac{d}{dt}\mathbf{r}(t)\right]_{\text{radial}} = \frac{2f}{c}\left\{\frac{d}{dt}\left(R_t \times R_{init} \times [x, y, z - z_0]^T\right)\right\} \times \mathbf{n}$$

$$= \frac{2f\omega}{c}\left\{\left(\hat{E}\cos\omega t + \hat{E}^2\sin\omega t\right) \cdot R_{init} \cdot [x, y, z - z_0]^T\right\} \cdot \mathbf{n} \tag{7}$$

2.3. Model of Multi-Target

The echo of multi-target with multi-scatters has complex and multi-component form, whose baseband signal can be modeled below:

$$S(t) = \sum_m \sum_n \rho_{mn} e^{\left(j2\pi f \frac{2r_{mn}(t)}{c}\right)} \tag{8}$$

where f is the carrier frequency of the narrowband radar, ρ_{mn} the echo intensity of the nth scatterer on the mth target, and $r_{mn}(t)$ the distance between the corresponding scatter and radar on time t. Then the Doppler frequency shift of the target is expressed as follows:

$$f_D = \frac{1}{2\pi}\frac{d\left(2\pi f \frac{2r_{mn}(t)}{c}\right)}{dt} = \frac{2f}{c}\frac{d}{dt}r_{mn}(t) \tag{9}$$

3. OCCLUSION EFFECT

Section 2 derived micro-Doppler caused by corresponding scattering centers, establishing micro motion model of spatial target without considering occlusion effect. When the radar line of sight failed to irradiate the scattering centers in the process of target micro motion, the scattering centers would not produce a modulated radar echo, which is defined as occlusion effect. RCS values of these three scattering centers P_1, P_2, P_3 in Fig. 1, σ_1, σ_2, σ_3, respectively, were

$$\sqrt{\sigma_1} = \frac{\sin(\pi/n)}{n}\sqrt{\frac{a}{k_0 \sin\theta}}\left[\left(\cos\frac{\pi}{n} - 1\right)^{-1} \mp \left(\cos\frac{\pi}{n} - \cos\frac{3\pi - 2\theta}{n}\right)^{-1}\right] \tag{10}$$

$$\sqrt{\sigma_2} = \begin{cases} l\dfrac{\sin(\pi/n)}{n}\sqrt{\dfrac{a}{k_0 \sin\theta}}\left[\left(\cos\dfrac{\pi}{n} - 1\right)^{-1} \pm \left(\cos\dfrac{\pi}{n} - \cos\dfrac{3\pi + 2\theta}{n}\right)^{-1}\right] & 0 < \theta \leq \gamma \\ 0 & \gamma < \theta \leq \pi/2 \\ \dfrac{\sin(\pi/n)}{n}\sqrt{\dfrac{a}{k_0 \sin\theta}}\left[\left(\cos\dfrac{\pi}{n} - 1\right)^{-1} \mp \left(\cos\dfrac{\pi}{n} - \cos\dfrac{\pi - 2\theta}{n}\right)^{-1}\right] & \theta > \pi/2 \end{cases} \tag{11}$$

$$\sqrt{\sigma_3} = \begin{cases} \sqrt{\pi}b\left[1 - \dfrac{\sin\left[2k_0 b\left(1 - \sin\gamma\right)\right]}{k_0 b\cos^2\gamma}\right]^{1/2} & \theta = 0 \\ \sqrt{\pi}b & 0 < \theta \leq \pi/2 - \gamma \\ 0 & \theta > \pi/2 - \gamma \end{cases} \tag{12}$$

where $n = 1.5 + \gamma\pi$, and γ and θ are the attitude angle and half cone angle respectively as indicated in Fig. 2.

From the analysis of formulas (10)–(12), attitude angle decides whether the three scattering points are obscured (RCS values equal to zero). Anechoic chamber experimental data also reflect the real relationship. The minimum size of the cone has central axis $h = 0.1\,\text{m}$, the bottom radius $r = 0.05\,\text{m}$, so the half cone angle $\gamma = \arctan(r/h) = 26.6°$. Under the theory, the attitude angles are $0°$, $15°$, $30°$, $90°$, respectively, and the numbers of scattering centers mainly on the smallest cone are 3, 3, 2, 1, respectively. Experimental results match theoretical analysis, illustrating that the number of scattering points on the cone target varies with target micro motion, i.e., occlusion effect does exist.

The change of attitude angle caused by cone target micro-motion can be calculated by the following method. The unit vector is $\vec{n} = [\cos\alpha\cos\beta,\ \sin\alpha\cos\beta,\ \sin\beta]^T$. In the initial time and under the radar reference coordinate, α_P, β_P, 0 are denoted as the yaw angle, pitch angle, and roll angle of the symmetry axis of cone target, respectively, then its unit vector is $\mathbf{n}_p(0) = [\cos\alpha_P\cos\beta_P,\ \sin\alpha_P\cos\beta_P,\ \sin\beta_P]^T$. In moment t, unit vector of the target axis is:

$$\mathbf{n}_p(t) = \mathbf{R}_t\mathbf{R}_{init}\mathbf{n}_p(0) \tag{13}$$

Vector angle formula $\mathbf{n} \cdot \mathbf{n}_p(t) = |\mathbf{n}|\,|\mathbf{n}_p(t)|\cos(\theta(t))$, where $\theta(t)$ is the attitude angle of cone target with micro motion. Then

$$\theta(t) = \arccos\left(\frac{\mathbf{n} \cdot \mathbf{n}_p(t)}{|\mathbf{n}|\,|\mathbf{n}_p(t)|}\right) \tag{14}$$

Reflected in the time-frequency characteristics, one or a few discrete time-frequency curves are not continuous.

4. INSTANTANEOUS FREQUENCY EXTRACTION

The frequency plane projection of the ideal time-frequency distribution is the instantaneous frequency curve, while the actual time-frequency distribution due to the limitation of the uncertainty principle cannot be focused in time and frequency domain at the same time. Thus when the ideal time-frequency distribution is in the frequency plane projection of the instantaneous frequency curve, the actual time-frequency distribution due to the limitation of the uncertainty principle cannot be reached in time and frequency focus. Extracting instantaneous frequency is the key to parameter estimation. The following two methods can effectively extract the instantaneous frequency.

4.1. The Local Maximum Value Selection Method

When there are multiple scatters on the target, the radar echo signal has multiple components. And STFT distribution peak projection of each component is the instantaneous frequency. Since the time-frequency map consists of several time-frequency intertwined curves, peak detection method and first order time conditional moment method proposed in [11] have been unable to extract the instantaneous frequency of each component (corresponding to each scattering point).

Discrete STFT distribution $\text{STFT}(m, k)$ of the signal is a matrix which has M rows and N columns, where N is the discrete number of coherent processing time. Ideally, for each column of the matrix, there exist maxima corresponding to the number of components (i.e., corresponding to the instantaneous frequency of each component). However, due to the presence of side lobes caused by random noise and window function, the number of maxima is far more than that of components. Fortunately, the random noise is uniformly distributed in the frequency domain, and when SNR is small, the noise will not cause a great impact on the time-frequency diagram. Gao [7] removed noise effect efficiently utilizing an image processing method. Meanwhile, side lobes caused by window function are small relative to main lobe. Through the establishment of the threshold, obtaining maximum values of those greater than the threshold to find the instantaneous frequency of each component is possible. This is how the local maximum value selection method works.

Mathematically instantaneous frequency estimation is expressed as:

$$\hat{f}_{mD}^{(k)}(j) = \arg_{k} \left\{ \text{Peak}[\text{STFT}_{M \times N}(:, j)] \right\} \tag{15}$$

where $\hat{f}_{mD}^{(k)}(j)$ represents the time j and component k of the micro-Doppler frequency estimation (k is no more than the number of scattered points and from 1 to N), $\text{STFT}_{M \times N}(:, j)$ the column j of the matrix, and $\arg(\cdot)$ the argument. And peak[] denotes the operation of selecting the maxima in the matrix.

Threshold selection is related to SNR and the width of the window function. Heisenberg uncertainty principle points out that for a given signal, the product of time width and frequency is a constant, namely $\Delta_t \Delta_f = \text{const}$, where Δ_t and Δ_f are time width and frequency width, respectively. const represents the constant (taken generally 1). Set the amplitude of target echo signal $x(n)$, $n = 0, 1, \ldots, L - 1$ to A; the width of Hamming window $g(n)(n = 0, 1, \ldots, P - 1)$ is P. After taking DFT of Q points, the maximum amplitude is set to B. Then $\Delta_t = P/L$, assuming that const $= 1$, $\Delta_f = L/P$. It is obtained that the percentage of Δ_f in the entire width of the frequency domain is $\eta = L/(PQ)$.

It is known that noise standard deviation satisfies the equation: $\sigma = A \times 10^{(\text{SNR}/10)}$. For Gaussian random variable X with zero mean and standard deviation σ, $p\{-3\sigma < X < 3\sigma\} = 0.9974$, $p\{-4\sigma < X < 4\sigma\} = 0.99999$. Therefore, noise amplitudes are almost all less than 4σ. After taking DFT of Q points, its magnitude is less than $4B \times 10^{(\text{SNR}/10)}$, where $\eta = 1$.

Set the maximum peak E of column (i.e., at some time DFT) after taking STFT of total return (target + noise), then the threshold is expressed as:

$$\text{threshold} = \frac{4 \times 10^{(\text{SNR}/10)}}{L/P + 4 \times 10^{(\text{SNR}/10)}} E \tag{16}$$

The algorithm flow of Maxima selection method is as follows:

 (i) Take STFT of echo signal (including noise) with multiple scatter to obtain transform frequency diagram;

 (ii) Obtain the threshold value based on the width of the window function and SNR;

 (iii) Set the above threshold value and filter out noise and side lobes in the time-frequency map;

 (iv) Obtain instantaneous frequency by searching the maxima.

4.2. The Method of Extract the Central Location

The frequencies dispersed along the center frequency (i.e., the instantaneous frequency) to both sides. And each frequency component concentrated in a certain period of matrix column vector. Thus, select

the value of the data segment in the middle position as an estimate of instantaneous frequency which is the principle of the center position extraction method.

Mathematically instantaneous frequency estimation is expressed as:

$$\hat{f}_{mD}^{(k)}(j) = \arg_k \left\{ \text{STFT}_{M \times N} \left[\left(i_0^{(k)} + \left| \frac{i_1^{(k)} - i_0^{(k)}}{2} \right| \right), j \right] \right\}$$

$$\begin{cases} \text{STFT}_{M \times N} \left(i_0^{(k)}, j \right) > \text{threshold}; \\ \text{STFT}_{M \times N} \left(i_0^{(k)} - 1, j \right) < \text{threshold} \\ \text{STFT}_{M \times N} \left(i_1^{(k)}, j \right) > \text{threshold}; \\ \text{STFT}_{M \times N} \left(i_1^{(k)} + 1, j \right) < \text{threshold} \end{cases} \tag{17}$$

where $\| \, \|$ indicates the rounding operation, and the threshold is obtained from (16).

DFT transform of the signal is symmetrical to the center frequency, and the above two methods are essentially the same. But the latter has its unique advantages. When the noise value of some moment is included in the range $-4\sigma < X < 4\sigma$, singular peak point will appear in the data. At this point, the first method fails while the later one will skip that point. However, the Central location extraction algorithm is not perfect either. When the difference between $i_1^{(k)}$ and $i_0^{(k)}$ is an odd number, the instantaneous frequency estimated and obtained by formula (17) will shift backward one frequency point, which results in frequency hopping, i.e., the discontinuous of the estimated values.

Central location extraction algorithm steps are as follows:

(i) The same as (i) (ii) (iii) in local maxima selection method.

(ii) Find the instantaneous frequency obtained through the center position.

5. SIMULATION DEMONSTRATION

Assuming that radar works in the X-band, carrier frequency and pulse repetition frequency are $f = 10\,\text{GHz}$, PRF $= 1024\,\text{Hz}$, respectively. Pulse width is $\tau = 1\,\mu\text{s}$. Centroid position in the radar coordinate system is $(U = 1000\,\text{m}, V = 5000\,\text{m}, W = 5000\,\text{m})$. The initial rotation angles are $\phi = 30°$, $\theta = 30°$, $\psi = 45°$. Precession angular velocity is $\omega = 4\pi\,(\text{rad/s})$. Azimuth angle and pitch angle are $\alpha_N = 60°$ and $\beta_N = 45°$, respectively. The point $S(x = 0\,\text{m}, y = 0\,\text{m}, z = -1\,\text{m})$ is in the axis. There are three scatters on the cone target: point P_0 which coincides with point S, point $P_1(x = 0.5\,\text{m}, y = 0.6\,\text{m}, z = 1.0\,\text{m})$, and point $P_2(x = -0.5\,\text{m}, y = -0.6\,\text{m}, z = -1.0\,\text{m})$. And target radial velocity is zero [20].
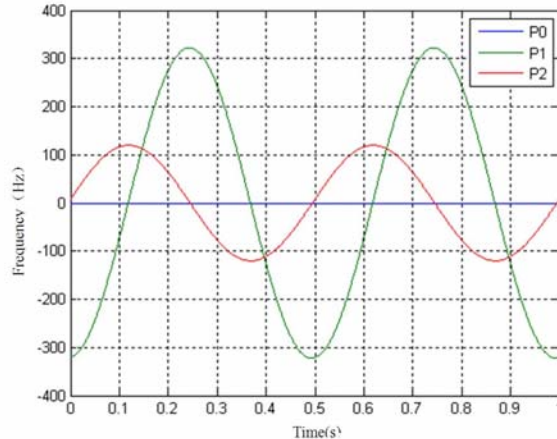

Figure 3. The Micro-Doppler theoretical curve.

5.1. Micro-Doppler Theoretical Curve

By (7), micro-Doppler curves of target are as shown in Fig. 3.

5.2. Time-Frequency Analysis Curve

For the echo with three scatters, we analyze it utilizing STFT where Hamming window function was adopted. Then two cases which are echo with noise (SNR $= -3$ dB, -10 dB), respectively, were analyzed and simulated. Fig. 4 and Fig. 5 respectively are the corresponding time-frequency analysis curves.

As can be seen from Fig. 4, the coning period is $T = 0.5$ which matches the actual one ($\omega = 4\pi$, then the period is 0.5 s). Comparing Fig. 4(c), Fig. 4(d) with Fig. 3, it can be seen that the extraction curve is substantially identical to the theoretical one. Paying attention again to Fig. 4(c), Fig. 4(d), one of the curves in the map obtained by utilizing the center position extraction method appears frequency hopping.

As can be observed from Fig. 4, when the SNR is large, noise has little effect on the time-frequency map. After de-noising by image processing, both methods can effectively extract the instantaneous frequency matching the curve in Fig. 3 basically.

As can be observed from Fig. 5, in the case of small SNR, time frequency map has been completely contaminated by noise. The image processing method of de-noising fails.
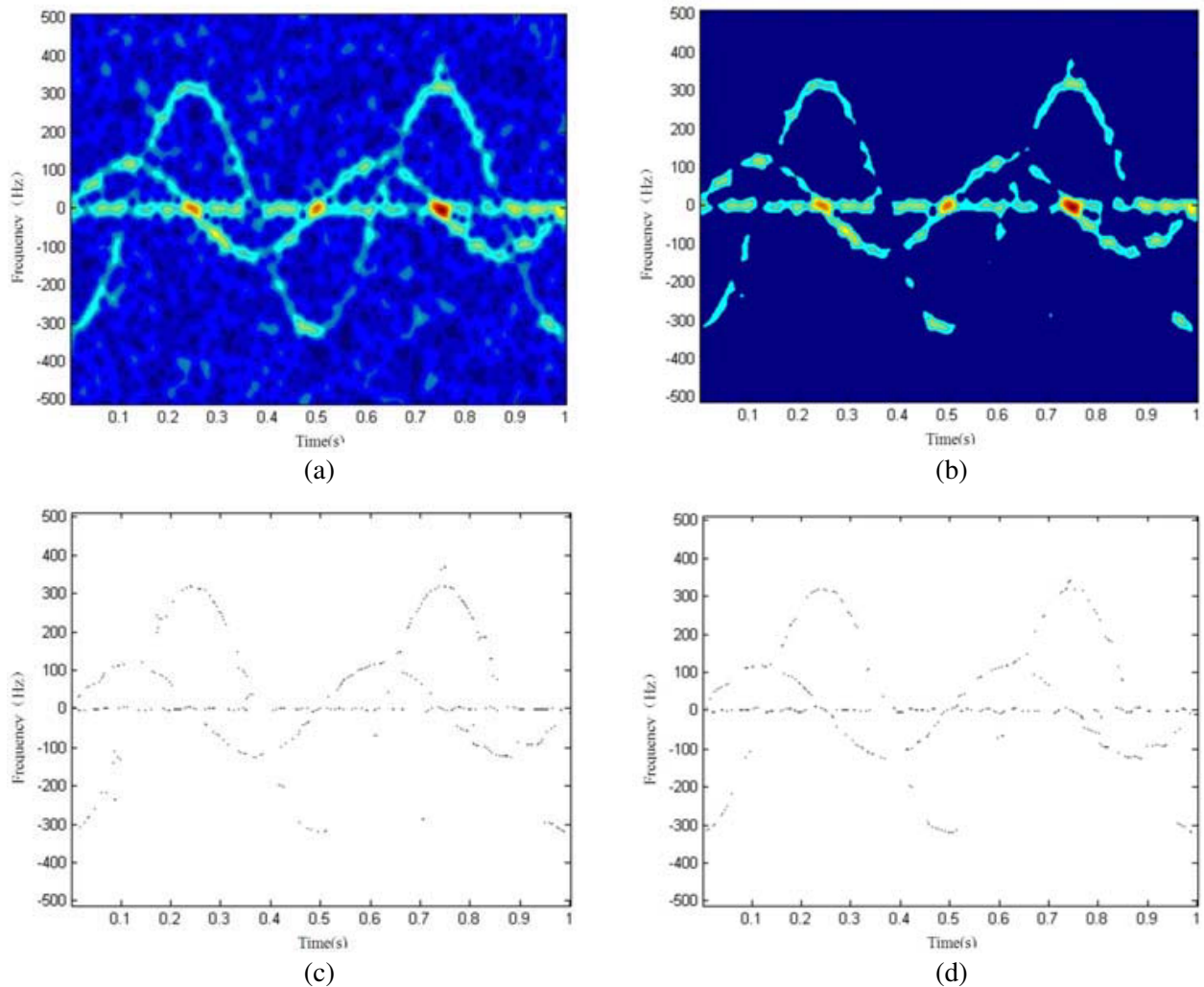

(a)

(b)

(c)

(d)

Figure 4. SNR $= -3$ dB.

(a)

(b)

Figure 5. SNR $= -10$ dB.

(a)

(b)

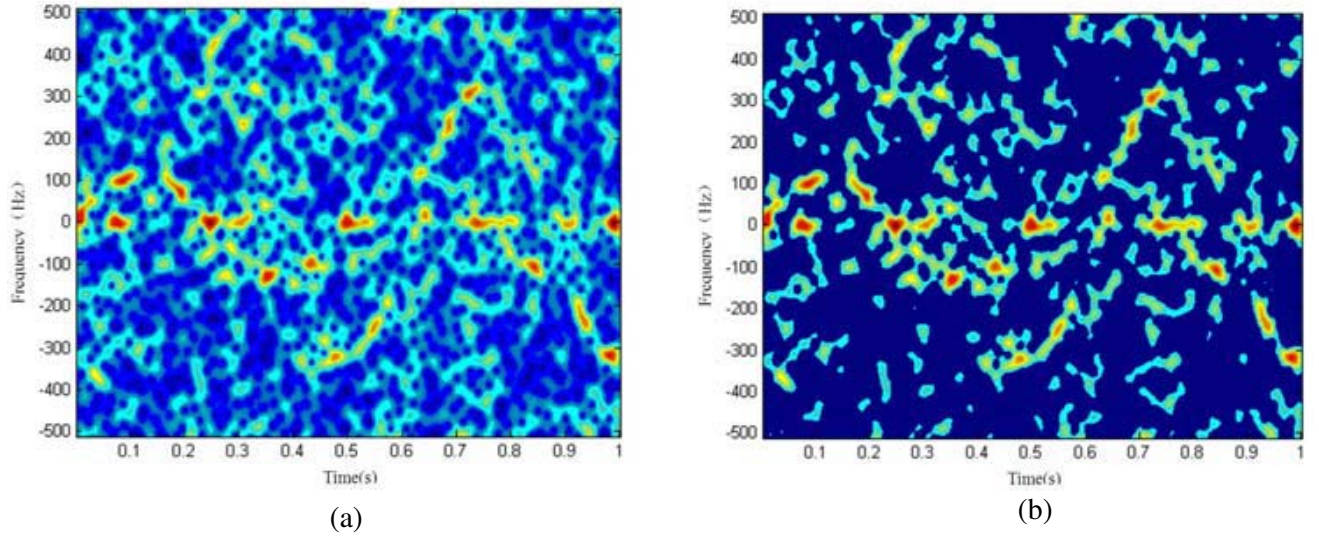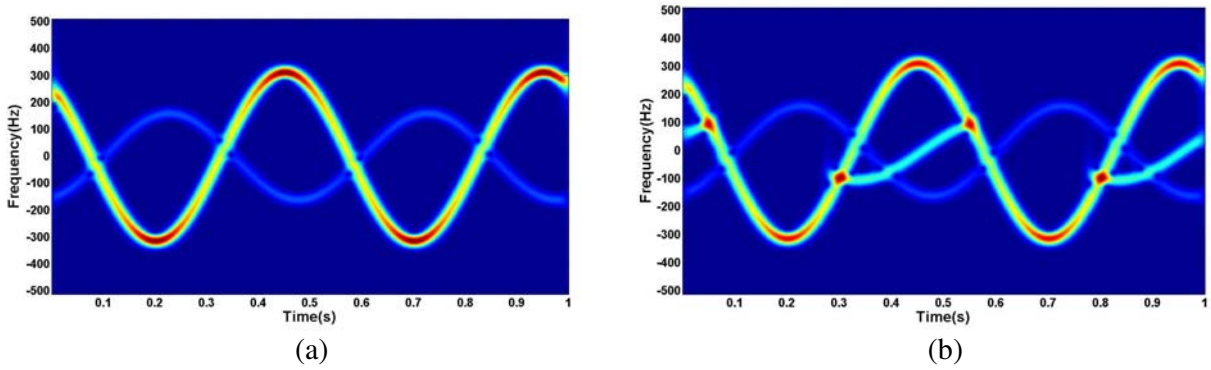**Figure 6.** Occlusion effect.

5.3. Occlusion Effect

Assume that the spinning angular velocity of the flat-bottomed cone target is $(0, 0, \pi)$ and half cone angle is $26.6°$, while the azimuth and elevation angles of the target symmetry axis are $(70°, 70°)$ or $(45°, 45°)$ under the target coordination. There exist three scatters on the target, which are $P_1(1.0\,\text{m}, 1.0\,\text{m}, -1.0\,\text{m})$, $P_2(-1.0\,\text{m}, -1.0\,\text{m}, -1.0\,\text{m})$ and $P_3(0\,\text{m}, 0\,\text{m}, 1\,\text{m})$. The rotation angle between the two coordinations on the target is $(30°, 20°, 20°)$. Other parameters are the same as those in Case A.

When the azimuth and elevation angles of the target symmetry axis are $(70°, 70°)$, posture angle change range is from $32°$ to $58°$. RCS of P_2 equals zero according to (11), so only two scatters P_1, P_3 cause curses on Time Frequency map, as shown in Fig. 6(a), while the azimuth and elevation angles of the target symmetry axis are $(45°, 45°)$. Although all three scatters exist, intermittent time-frequency map appears due to occlusion effect (Fig. 6(b)).

5.4. Compare Viterbi Algorithm and the Local Maxima Selection Method

In this case, there are two flat-bottomed cone targets, but the radar parameters remain the same. And the first target is exactly the same one in Section 5.2. For the other one, its centroid position in the radar coordinate system is $(U = 1100\,\text{m}, V = 5000\,\text{m}, W = 5100\,\text{m})$. Its rotation angles are $(30°, 45°, 30°)$, and azimuth and elevation angles of the symmetry axis are $(60°, 60°)$. Both targets share
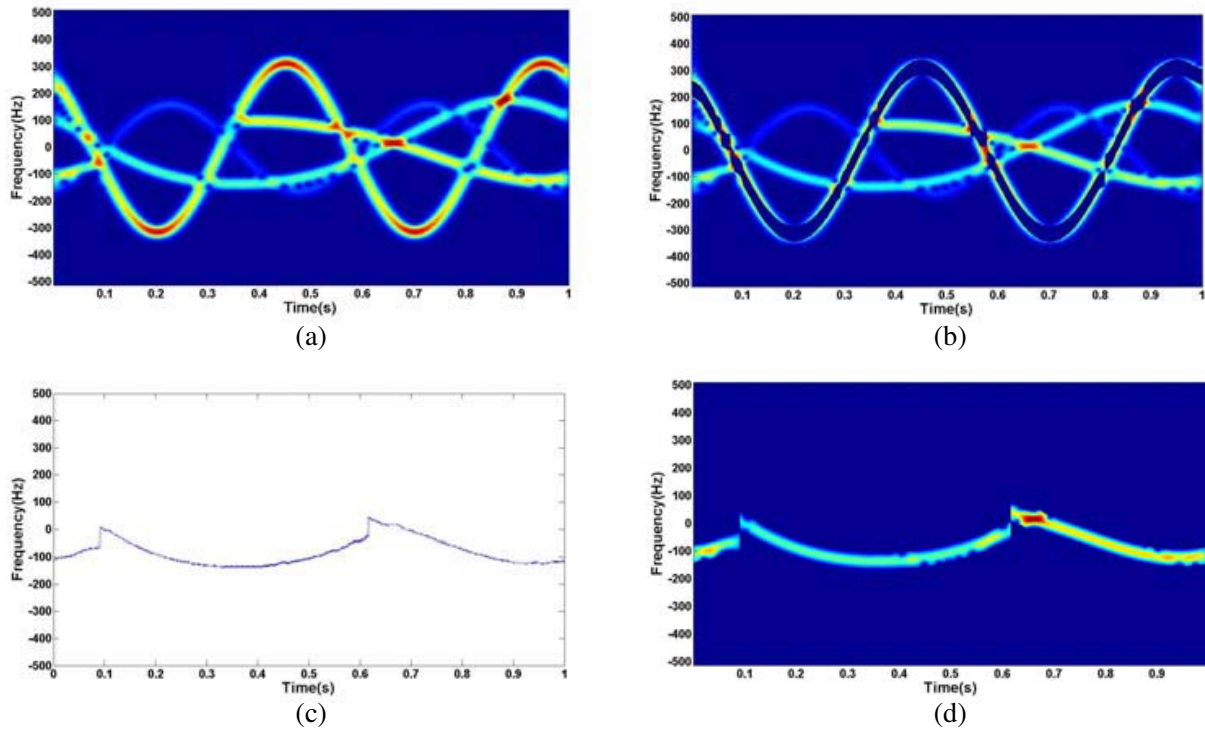
(a)

(b)

(c)

(d)

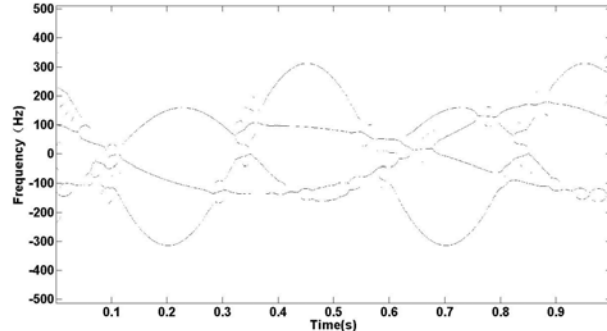**Figure 7.** The failure of Viterbi algorithm.

Figure 8. The result of proposed method on TF map with discontinuous points.

parameters of precession and spinning. But the latter also wobbles with precession with the first one. And its max angle of wobbling is $10°$, and wobbling angular velocity is 2π (rad/s). In the process of Viterbi Algorithm [19], we set $m = 5$, $c = 3$, $\Delta = 2$, $B = 60$.

The time frequency map involving occlusion effect is shown in Fig. 7(a). The map after eliminating the strongest components of the time frequency distribution using Viterbi Algorithm is shown in Fig. 7(b). It is not difficult to find that the strongest component should be the interrupted curve. Fig. 7(c) and Fig. 7(d) further demonstrate the error of separation due to the tracking feature of Viterbi Algorithm.

Figure 8 is the result of local maxima selection method in the same scenario. Though there exist estimated deviation spectrogram crossings, it does not influence the recognition throughout the instantaneous frequency curves. For the presence of discontinuities in the frequency diagram, this method can still effectively extract the instantaneous frequency.

At least one vital conclusion was drawn from this case: Viterbi algorithm for the separation of instantaneous frequency in discontinuous multi-component Spectrograms was not applicable.

6. CONCLUSIONS

Micro-Doppler signal instantaneous frequency extraction is the key to parameter estimation of targets with micro motions. It is vital to accurately obtain the instantaneous frequency. Beside the separation methods, existing methods can only extract single instantaneous frequency components of the signal. The two methods presented in this paper do not fail in the case of multi-component. When the signal to noise ratio is large, two methods are still valid. In the future work, we will focus on the methods divided by parametrical and nonparametric ones. To solve the problem caused by occlusion effect, a hybrid method will be exploited.

REFERENCES

1. Chen, V. C., "Analysis of radar Micro-Doppler signature with time-frequency transform," *Proc. of the Tenth IEEE Workshop on Statistical Signal and Array Processing*, 463–466, 2000.
2. Chen, V. C., "Micro-Doppler effect in radar: Phenomenon, model and simulation study," *IEEE Trans. AES*, Vol. 42, No. 1, 2–21, 2006.
3. Yong, C., "Radar target feature extraction fretting research," *Journal Title Abbreviation*, 2006.
4. Zhuang, Z.-W., "Fretting characteristics of the target research progress," *Journal of Electronics*, Vol. 35, No. 3, 520–527, 2007.
5. Yong, C., "Fretting target Doppler spectral analysis and parameter estimation," *Signal Processing*, Vol. 24, No. 1, 1–6, 2008.
6. Gao, H., "Other Micro-Doppler wobble cone objective analysis and extraction," *Journal of Electronics*, Vol. 36, No. 12, 2497–2502, 2008.
7. Gao, H., "Beams and other ballistic missile target fretting characteristics and simulation of Micro-Doppler analysis," *System Simulation*, Vol. 21, No. 4, 954–961, 2009.
8. Liu, Y. X., "Instantaneous frequency estimation of multi-component signal based on complex-argument distribution," *IEEE International Conference on Signal Processing*, 2010.
9. Liu, Y., "Research fretting characteristics of the target. Technology review," *Journal Title Abbreviation*, Vol. 29, No. 22, 73–79, 2011.
10. Chen, V. C., *The Micro-Doppler Effect in Radar*, Artech House, Boston, 2011.
11. Yong, C., "Micro-Doppler analysis and parameter estimation," *Infrared and Millimeter Wave Newspaper*, Vol. 34, No. 10, 360–363, 2006.
12. Li, J. L., "Application of adaptive chirplet representation for ISAR feature extraction form targets with rotating parts," *IEEE Proc. Radar Sonar Navig.*, Vol. 4, No. 150, 284–291, 2003.
13. Stankovic, L. D., "Separation of target rigid body and Micro-Doppler effects in ISAR imaging," *IEEE Trans. Aerosp. Electron. Syst.*, Vol. 4, No. 42, 1496–1506, 2006.
14. Thayaparan, T. S., "Analysis of radar Micro-Doppler signatures from experimental helicopter and human data," *IEEE Proc. Radar Sonar Navig.*, Vol. 4, No. 1, 289–299, 2007.
15. Zhang, Q. Y., "Imaging of a moving target with rotating parts based on the Hough transform," *IEEE Trans. Geosci. Remote Sens.*, Vol. 46, No. 1, 291–299, 2008.
16. Bai, X. R., "Imaging of micromotion targets with rotating parts based on empirical mode decomposition," *IEEE Trans. Geosci. Remote Sens.*, Vol. 46, No. 11, 3514–3523, 2008.
17. Thayaparan, T. S., "Micro-Doppler analysis of a rotating target in synthetic aperture radar," *IET Signal Process*, Vol. 4, No. 3, 245–255, 2010.
18. Lu, Y. L., "Radar Micro-Doppler signature analysis with HHT," *IEEE Trans. Aerosp. Electron. Syst.*, Vol. 46, No. 2, 929–938, 2010.
19. Li, P., D.-C. Wang, and L. Wang, "Separation of Micro-Doppler signals based on time frequency filter and Viterbi algorithm," *Signal, Image and Video Processing*, 2011.
20. Mencia-Oliva, B. G., "Low-cost CW-LFM radar sensor at 100 GHz," *IEEE Trans. Microw. Theory Techn.*, Vol. 61, No. 2, 986–998, 2013.